J Mol Model (2015) 21: 9
DOI 10.1007/s00894-014-2564-2

ORIGINAL PAPER

Molecular dynamics simulation of melting and crystallization processes of polyethylene clusters confined in armchair single-walled carbon nanotubes

Zhou Zhou · Jinjian Wang · Xiaolei Zhu · Xiaohua Lu · Wenwen Guan · Yuchen Yang

Received: 2 October 2014 / Accepted: 14 December 2014 / Published online: 22 January 2015

Abstract The confined interaction is important to understand the melting and crystallization of polymers within single-wall carbon tube (SWNT). However, it is difficult for us to observe this interaction. In the current work, the structures and behaviors of melting and crystallization for polyethylene (PE) clusters confined in armchair single-walled carbon nanotubes ((n, n)-SWNTs) are investigated and examined based on molecular dynamics (MD) simulations. The nonbonded energies, structures, Lindemman indices, radial density distributions, and diffusion coefficients are used to demonstrate the features of melting phase transition for PE clusters confined in (n,n)-SWNTs. The chain end-to-end distance (R_n) and chain end-to-end distribution are used to examine the flexibility of the PE chain confined in SWNT. The global orientational order parameter (P_2) is employed to reveal the order degree of whole PE polymer. The effect of polymerization degree on melting temperature and the influence of SWNT chirality on structure of PE cluster are examined and discussed. Results demonstrate that within the confined environment of SWNT, PE clusters adopt novel co-axial crystalline layer structure, in which parallel chains of each layer are approximately vertical to tube axis. The disordered-ordered transformation of PE chains in each layer is an important structural feature for crystallization of confined PE clusters. SWNTs have a considerable effect on the structures and stabilities of the confined PE clusters.

Keywords Carbon nanotube · Crystallization · Melting · Molecular dynamics simulation · Polyethylene cluster

Introduction

It is well known that the properties of polymers can be adjusted very easily because monomers, branching, tacticity, blends, copolymers, and composites [1, 2] can be selected. Crystallization of polymers with a regular ordered chemical structure is one of the most important processes in materials science and condensed-matter physics since the crystal growth and the final properties of the crystalline polymer will be controlled by the polymer crystallization [3]. In order to design favorable structures of crystalline polymers, clearly, it is necessary to know much more about the molecular mechanism of polymer crystallization. Therefore, the polymer crystallization has been the topic of many experimental and computational studies [4–12]. The complicated structures of polymers lead to that the investigation on the polymer crystallization is very challenging. The molecular dynamics (MD) simulation has been considered as a powerful tool for revealing the mechanism of polymer crystallization [4–12].

Recently, much attention has been devoted to inducing crystallization of polymers using substrates [13–21], in which the interfaces play key roles in inducing polymer crystallization. Many scientists have experimentally and theoretically investigated the structures, orientation, and crystallization mechanism during inducing crystallization of polymers with single-wall carbon tube (SWNT) or graphene nanosheet as substrate [3–19], which have made considerable progress in the investigations on polymer crystallization. For example, carbon nanotube (CNT)-induced polymer crystallization has been systematically investigated by experiments and

Electronic supplementary material The online version of this article (doi:10.1007/s00894-014-2564-2) contains supplementary material, which is available to authorized users.

Z. Zhou · J. Wang · X. Zhu (✉) · X. Lu (✉) · W. Guan · Y. Yang
State Key Laboratory of Materials-Oriented Chemical Engineering, College of Chemistry and Chemical Engineering, Nanjing Tech University, Nanjing 210009, China
e-mail: xlzhu@njtech.edu.cn
e-mail: xhlu@njtech.edu.cn

molecular dynamics simulations [14–20]. Wei et al. carried out MD simulations on the alkane chain crystallization around the CNT [14, 15]. The results showed that the alkane chain crystallization is closely related to the length of alkane chain and CNT chirality. Li et al. demonstrated that polymeric materials can form single crystals on the surfaces of CNTs and carbon nanofibers (CNFs) [16–18]. Hu et al. proposed surface-induced conformational order (SICO) to explain interchain interaction [19]. Recently, there have been some interesting reports about surface-inducing studies, for example, the polymers with complex chemical structures have been induced by the outer surfaces of carbon nanotube [22] or nanoparticle [23]. Results have demonstrated that that polymer at the CNT (or nanoparticle) interface organizes into layered structures. Due to the complex chemical structures of the polymers and weaker outer-surface inducing effect, it is difficult to induce crystallization of polymers in their works. Yang et al. found that CNT has a stronger ability to induce the polymer crystallization than graphene nanosheet [3], supporting the experimental observation at molecular level [16, 24].

Despite the existing studies as mentioned above, there is a lack of systematical investigation on the melting and crystallization processes of polymers confined within single-wall carbon tube (SWNT). Polyethylene (PE) is an example of a polymer that has many industrial applications such as plastic films and sheets, a wide variety of containers, kitchenware, and tubing [25]. On the other hand, since the branches of polymers will affect the crystallization process [26], PE possesses a relatively simple structure without branches, which avoids the above problem. Thus, it will be convenient for us to investigate polymer inner-surface-induced crystallization within the confined environment of SWNT. Herein, we first perform MD simulations to investigate the structures, melting, and crystallization phase transitions on PE clusters confined in (n,n)-SWNTs. The confined environment of SWNT leads to the interesting multishell structure of PE clusters, in which the parallel chains of each layer are perpendicular to tube axis. Some important features of melting and crystallization for confined PE clusters are examined and revealed, which are valuable for further experimental studies.

Computational details

We investigate and reveal melting and freezing behaviors of PE clusters confined in armchair single-wall carbon tube ((n, n)-SWNT) with n=30, 40, 50, and 60 based on MD simulations. The corresponding diameters of (n,n)-SWNTs are 40.7, 54.2, 67.8, and 81.4 Å, respectively. Each system includes a PE cluster filled in the carbon tube and an infinitely long SWNT (simulated by a box of length 344.3 Å replicated using periodic boundary conditions along the tube axis). In MD simulations, the PE clusters (the degree of polymerization (DP) is 15) include the number of chains (N) of 63, 166, 287, and 435, respectively (containing 1890, 4980, 8610, and 13050 united atoms, respectively) as shown in Table 1. For convenience, we distinguish the different systems by representing the degree of polymerization (DP), the number of chains (N), and the index n of the (n,n)-SWNT (PE (DP,N)-n), that is, the systems studied in this work are marked as PE (15,63)-30, PE (15,166)-40, PE (15,287)-50, PE (15,435)-60, respectively.

Molecular dynamics simulations are carried out on the above systems during the cooling and heating processes using LAMMPS software obtained from the Sandia National Laboratory [27] (http://lammps.sandia.gov/). In the current work, the united atom (UA) force field is used to describe the interactions of PE, in which each PE chain are made up of spherical beads, each accounting for a CH_2 united atom or CH_3 for the terminal bead. Each bead interacts via bonded and nonbonded potentials. The bonded potentials include the bond stretching energy (E_{bond}) for two adjacent beads, the bond angle bending energy (E_{angle}) among three adjacent beads. The nonbonded interactions ($E_{L\text{-}J}$) are described based on Lennard-Jones (L-J) 6–12 forces for all inter-molecular interactions between beads and for intra-molecular interactions between beads that are separated by four or more bonds. The cutoff is taken as 9.5 Å. The total energy E_{total} can be represented by:

$$E_{total} = E_{bond} + E_{angle} + E_{L-J} = \frac{1}{2}k_b(r-r_0)^2 + \frac{1}{2}k_\theta(\cos\theta_a - \cos\theta_0)^2 + 4\varepsilon\left[\left(\frac{\sigma}{r}\right)^{12} - \left(\frac{\sigma}{r}\right)^{6}\right], \quad (1)$$

where k_b=3.588e V Å^{-2}, r_0=1.520 Å, k_θ=9.332×10^{-2} eV and θ_0=180° as shown in reference [28]. σ and ε are the distance between two sites, the distance at zero energy (U_{LJ}=0), and the energy well depth, respectively. In MD simulation, SWNTs are approximately considered as the rigid superstructures of fixed atoms [29, 30]. The L-J potential parameters [31, 32] applied in MD simulations are listed in Table 2. In literature [33] and [34], for modeling melting/freezing of alkane/polymer, usually, there are two different methods to deal with CH_2 and CH_3 groups. One is that CH_2 and CH_3 groups are taken as the same beads in the non-bonded potential [33]. Another is that CH_2 and CH_3 groups are considered as two different beads in the non-bonded potential [34]. In the above two methods, CH_2 and CH_3 groups are taken as the same beads in bonded potential. In the UA model used in the current work, CH_2 and CH_3 groups are treated as approximately the same beads.

During phase transition simulations for the systems studied, the PE cluster inserted into the armchair SWNT is melted by bringing it to a temperature above 190 K for 8.0 ns. After that, a slow cooling run is performed from 190 to 50 K with

Table 1 Pore diameters (D) of (n,n)-SWNTs, degrees of polymerization (*DP*), number of chains (*N*), and total number of united atoms (M_{UA}) for the different systems simulated

Model No.	1	2	3	4	5	6
System	63PE-30	166PE-40	287PE-50	435PE-60	100PE-40	71PE-40
(n,n)	(30, 30)	(40, 40)	(50, 50)	(60, 60)	(40, 40)	(40, 40)
D (Å)	40.68	54.24	67.80	81.36	54.24	54.24
DP	15	15	15	15	25	35
N	63	166	287	435	100	71
M_{UA}	1890	4980	8610	13050	5000	4970

temperature step ΔT=10 K and time step Δt=2 fs. Each system is first simulated at constant temperature (NVT ensemble) for 4 ns and then simulated at constant energy (NVE ensemble) for 4 ns. For constant temperature MD simulations, in order to reach the desired temperature, velocities are rescaled at each step [35]. The final structure at 50 K obtained from the cooling process is taken as the initial configuration for the slow heating process. In the slow heating process, each confined PE cluster is heated from 50 to 190 K with a similar simulation method of cooling process. During each MD simulation, a structure is saved per 0.04 ns.

Results and discussion

Figure 1 shows the correlation of nonbonded energy with temperature for PE clusters filled in SWNTs during slow heating processes. As shown in Fig. 1, energy jumps in the nonbonded energy curves demonstrate the melting phase transitions of PE clusters. As shown in Fig. 1, PE (15,63), PE (15, 166), PE (15,287), and PE (15,435) clusters within SWNTs melt around 140, 150, 155, and 160 K, respectively. Results suggest that the melting temperatures of confined PE (PD,N) clusters tend to increase with cluster size as expected. Furthermore, the melting temperatures are lower than those (397–407 K) [36] of free bulk PE. The atomic cohesive energies [37] of free and confined PE (15,166) clusters are calculated and shown in Fig. 2 to reveal the confined effect of SWNT on the stability of PE clusters. Clearly, the cohesive energies of the confined PE (15,166) cluster is significantly lower than those of free PE (15,166) cluster, that is, the confined effect of SWNT significantly improves the thermal stability of PE (15,166) cluster. As mentioned above, the cohesive energies of confined PE cluster are lower than that of its free cluster.

Table 2 Potential parameters for Lennard-Jones potential used in MD simulations

Pairs	ε (10^{-3}, eV)	σ (Å)	Reference
CH_2-CH_2	4.250	3.94	[29]
CH_2-C_{SWNT}	2.412	3.4	[30]

However, the melting temperatures of confined PE clusters are lower than those of free bulk PE [36] as mentioned above. It is due to the fact that the confined PE clusters have lower dimension, the increase in melting point caused by the confined environment does not exceed that resulted from increasing of cluster size in free bulk, and free PE bulk has stable orthogonal crystal structure.

To examine the effect of polymerization degree on the melting temperatures of PE clusters, Fig. 3 demonstrates the relationship between melting temperature of confined PE cluster and the polymerization degree for PE (15,287)-40, PE (25, 100)-40, and PE (35,71)-40 (approximately including 5000 united atoms of PE, respectively), which reveals that the melting temperature increases with increasing of the polymerization degree as expected.

The structures of PE (DP,N)-40 systems at 50 K are represented in Fig. 4 to reveal structural features of confined PE clusters. It is found from Fig. 4 that the solid-like PE clusters confined in SWNTs adopt co-axial crystalline layer structures and the PE chains of each layer are parallel to each other and approximately perpendicular to the tube axis as shown in

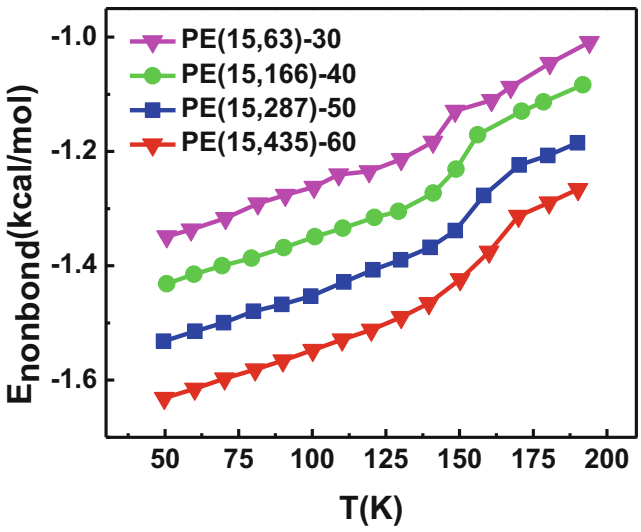

Fig. 1 Temperature dependence of nonbonded energy for PE clusters confined in (n,n)-SWNTs during heating process. The curves of PE (15,166)-40, PE (15,287)-50, and PE (15,435)-60 are shifted downward by 0.05, 0.15, and 0.25 kcal mol^{-1}, respectively

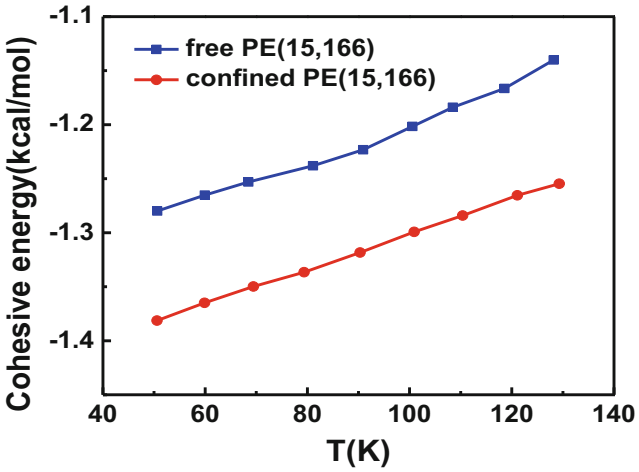

Fig. 2 Cohesive energies as a function of temperature for free and confined PE (15,166)

Fig. 5, which are different from the bulk structure of free PE polymer [36]. Clearly, the multishell structures of confined PE clusters are closely related to the confined environment of SWNT. The structure of confined PE (15,166) cluster is relatively more ordered than those of free PE cluster, suggesting that SWNT improves the stability of PE (15,166) cluster. Here, we have additionally performed the MD simulations on PE (15,166)-40 system with the UA potential including dihedral potential [38] and the completely flexible UA potential [39], respectively. After cooling down to 50 K, the structures obtained based on these two UA potentials represented in Figs. SI-1 (a) and SI-1 (b), respectively, are similar to the structure in Fig. 4. The above results reveal that three different

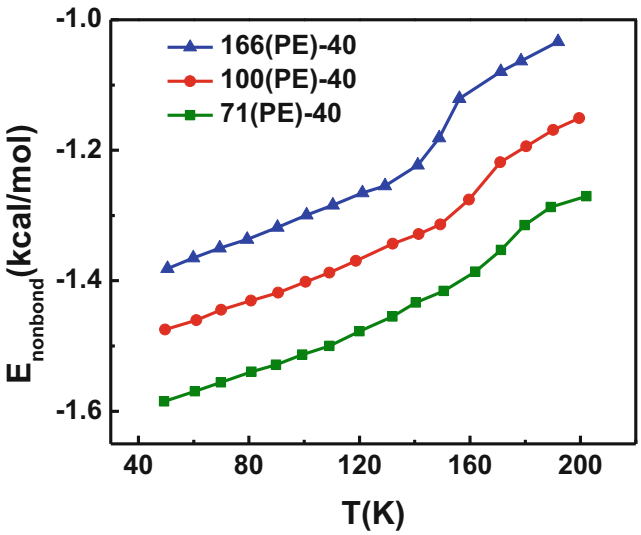

Fig. 3 The effect of polymerization degree on melting temperatures of PE clusters confined in SWNT for PE (15,287)-40,PE (25,100)-40, and PE (35,71)-40 (approximately including 5000 united atoms of PE, respectively). The curves of PE (25,100)-40 and PE (35,71)-40 are shifted downward by 0.1 and 0.2 kcal mol^{-1}, respectively, for clarity

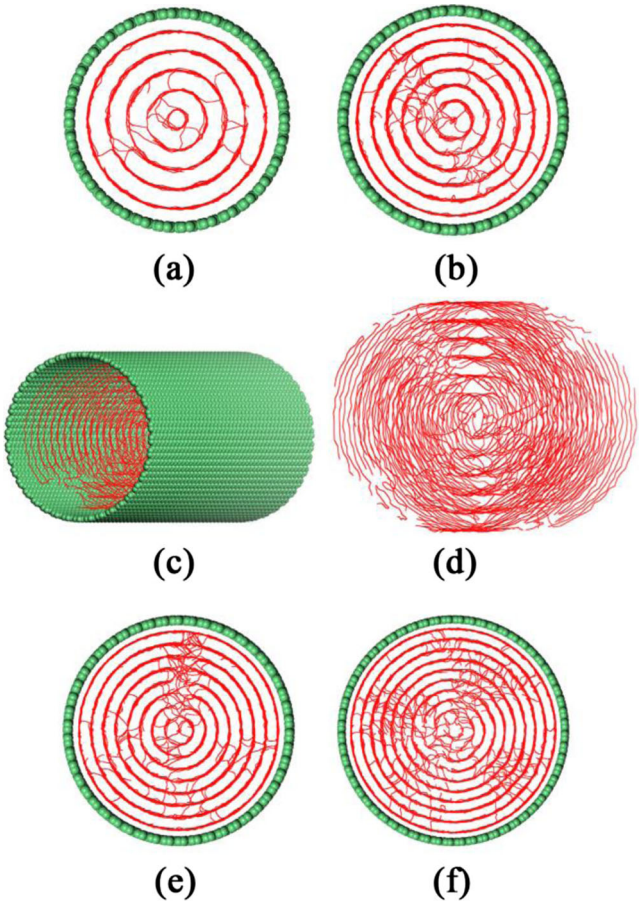

Fig. 4 Images of PE clusters confined in (n,n)-SWNTs at 50 K. **a** for PE (15,63)-30; **b**, **c**, and **d** for PE (15,166)-40; **e** for PE (15,287)-50; **f** for PE (15,435)-60. The *red lines and green balls* represent PE chains and the atoms of carbon tube, respectively

UA potentials [28, 38, 39] have similar influence the structure of PE (15,166) confined in SWNT. In order to explore the melting transformation process, we examine the structures of confined PE clusters during cooling and heating processes. During slow cooling and heating stages, the snapshots of PE (15,166) clusters inside SWNTs are displayed in Fig. 6. Before the melting temperature, the PE (15,166) clusters have

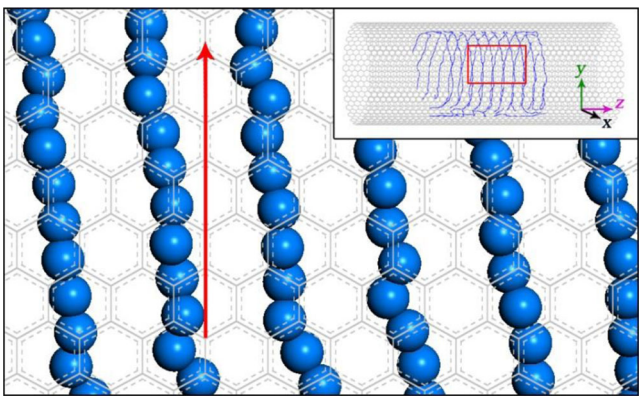

Fig. 5 Chain orietation for outmost-layer of PE (15,63) cluster at 50 K

multishell structures (Fig. 6c, d, e, and f) with ordered structure. After melting temperature, the PE (15,166) clusters possess random orientated structures (Fig. 6 (a and b, g and h). During quenching runs, the multishell structure of confined PE (15,166) cluster is also observed. Additionally, in order to examine the effect of SWNT chirality on the structure of PE clusters, the MD simulations on PE (15,63) clusters confined in (30, 30)-SWNT, (20, 39)-SWNT, and (52, 0)-SWNT, respectively, are performed. Figure SI-2 demonstrates that the structures of PE (15,63) clusters confined in three different SWNTs are similar, which is different from the results based on inducing crystallization out of tube by Wei et al.[14, 15].

The Lindemann indices [40] can be used to estimate phase transitions and reveal melting features of a cluster. Here, the confined PE cluster is divided into several shells in radial direction. The Lindemann index [40] of each layer δ_i is given by:

$$\delta_i = 2/(N_i(N_i-1))\sum_{j<k}\sqrt{\left\langle r_{jk}^2\right\rangle-\left\langle r_{jk}\right\rangle^2}/\left\langle r_{jk}\right\rangle, \quad (2)$$

where N_i is the number of atoms of the ith layer and r_{jk} represents the distance between united-atoms j and k. The Lindemman index for the confined PE (15,166) as a function of temperature is displayed in Fig. 7. As mentioned above, the solid PE (15,166) cluster includes seven co-axial crystalline layers. As shown in Fig. 7, although δ (second layer), δ (seventh layer), and δ (total) are close within the temperature ranges of 50–90 K and 170–190 K, within the temperature range of 90~170 K, δ (second layer) is considerably larger than δ (seventh layer) and δ (total). δ (second layer) first reaches 0.1 at about 130 K, revealing that the melting of PE (15,166) cluster starts from inner layers. δ (seven layer) reaches 0.1 at about 153 K, which is lower than the melting temperature of the confined PE (15,166). It can be ascribed to

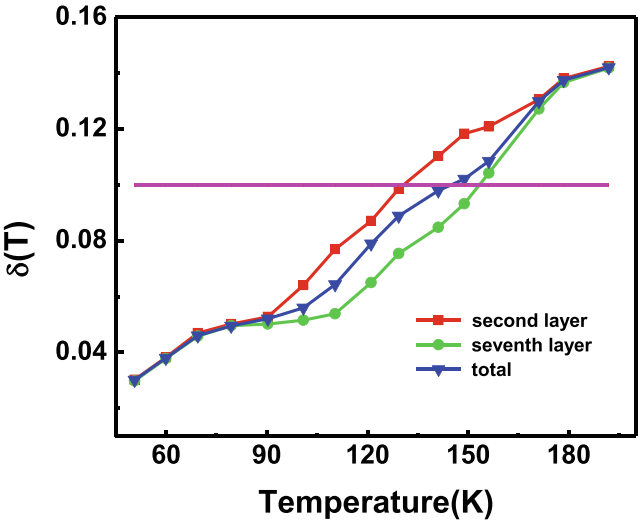

Fig. 7 Lindemann indices as a function of temperature for PE (15,166)-40

the following reasons. For PE (15,166) clusters confined in SWNT, the interactions between the surface atoms of PE (15,166) clusters and SWNTs are stronger and surface atoms around SWNT substrate have the lesser degree of freedom, which results in higher surface melting temperature for confined PE (15,166) cluster.

The averaged diffusion coefficients can also be applied to identify the melting transformation [41]. Figure SI-3 shows the averaged diffusion coefficients in PE (15,166)-40 during heating process calculated based on:

$$D = \frac{1}{6}\lim_{t\to\infty}\frac{d}{dt}\langle[r_i(t+t_0)-r_i(t_0)]\rangle, \quad (3)$$

where D is the self-diffusion coefficient, r_i (t) is the atomic position of the PE cluster. The bracket displays an ensemble

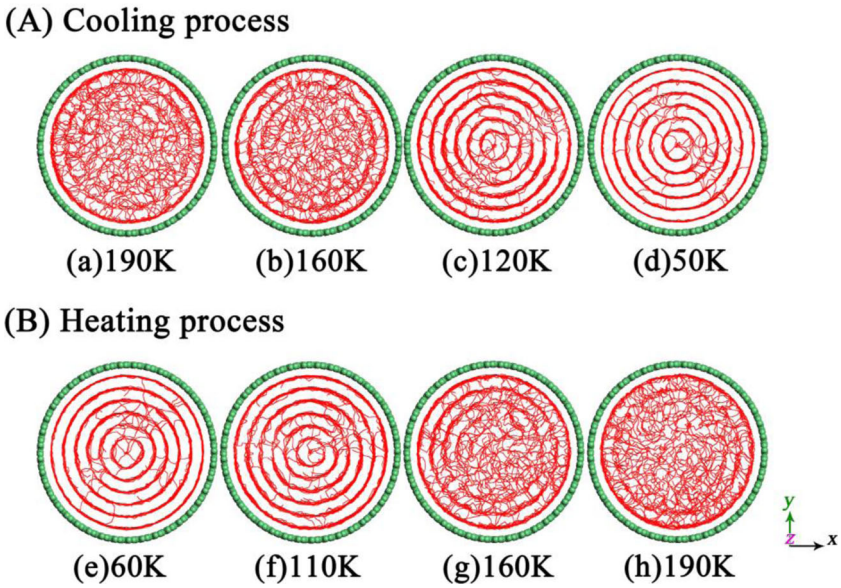

Fig. 6 Snapshots of PE (15, 166) clusters confined in (30,30)-SWNTs parallel to the tube axis of SWNTs at corresponding temperatures. **A** Cooling process ((**a**) 190 K, (**b**) 160 K, (**c**) 120 K, (**d**) 50 K); **B** Heating process ((**e**) 60 K, (**f**) 110 K, (**g**) 160 K, (**h**) 190 K). The red lines and green balls represent PE chains and the atoms of carbon tube, respectively

average. As shown in Fig. SI-3, the diffusion coefficients of the confined PE (15,166) slowly increase as temperature increases. However, near its melting temperature of 150 K, diffusion coefficients increase rapidly. It is due to the fact that at melting point (150 K), the confined PE (15,166) cluster undergoes the transformation from the crystal to melt, resulting in considerable increasing of diffusion coefficients.

In order to further understand the effects of the carbon nanotube substrate on the structures of PE (DP,N) clusters during heating and cooling processes, the radial density distributions of PE (15,166) confined in (40,40)-SWNTs at different temperatures have been analyzed and are represented in Fig. 8. The seven peaks on the radial density curve of the confined PE (15,166) cluster correspond to a seven-layer stacked structure before melting (Fig. 8 (a) 50 K, 110 K and (b) 50 K,110 K), which is consistent with the results of Fig. 6. It is worth noting that there exists a layering phenomenon in the melted PE (15, 166) within SWNT (Fig. 8 (a) 160 K,190 K, and Fig. 8 (b) 160 K, 190 K). Obviously, the layering stack structures of PE clusters confined in SWNT are attributed to the confined environment of SWNT. On the other hand, we also analyze the axial density distributions of PE (15,63)-30 and PE (15,287)-50 parallel to the tube axis at 50 K as shown in Fig. SI-4, which suggests that each of the axial density distributions includes some stable peaks and gradually decreases at two ends of the clusters with $|z|$ increasing, which is in agreement with the results of Fig. 8. Also, the gradual dropping of the axial density can be attributed to the capping effect.

In order to examine the flexibility of the PE chain confined in SWNT, the chain end-to-end distance (R_n), and chain end-to-end distribution [42] are analyzed and discussed as follows. Figure 9 illustrates the temperature dependence of averaged end-to end distances<r_{ee}>of PE (15,166) cluster confined in (40,40)-SWNT during heating and cooling processes, in which during cooling/heating process, the sudden changes on<r_{ee}>−T curves correspond to freezing/melting transformations of the confined PE (15,166)-40. Obviously, in high temperature region, the stronger interchain interactions lead to its disordered structure. Figures 10a and b represent the probability distribution of the averaged end-to-end distance of the confined PE (15,166) cluster during heating and cooling processes, respectively. As shown in Fig. 10a, a major peak appears at ~34 Å for crystalline state of the confined PE (15,166) cluster during heating process and moves to smaller distance (~19 Å) upon melting owing to enwinding of polymer chain as expected. In addition, r_{ee} distribution curves in Fig. 10 a adopt approximately Gaussian-like distribution above 150 K. The features of Fig. 9b are similar to those of Fig. 10a.

The global orientational order parameter P_2 [43] is often applied to examine the order degree of whole polymer during

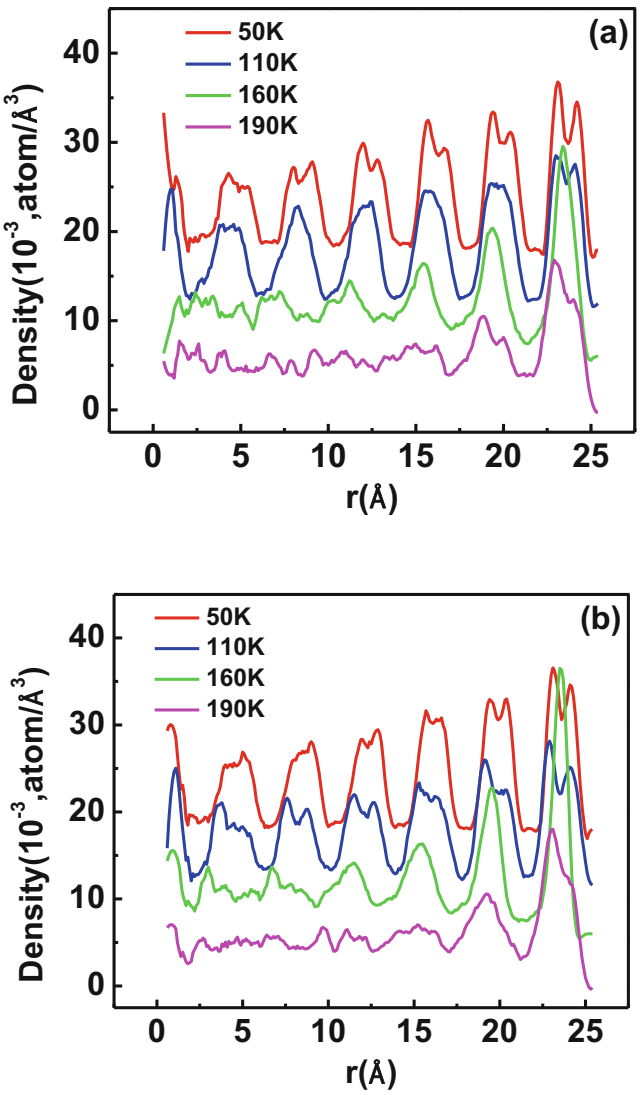

Fig. 8 Radial density function for the confined PE (15,166) during the cooling (**a**) and heating (**b**) processes. The curves at 160, 110, and 50 K are shifted upward by 0.006, 0.012, and 0.018 atom/Å^{-3}, respectively

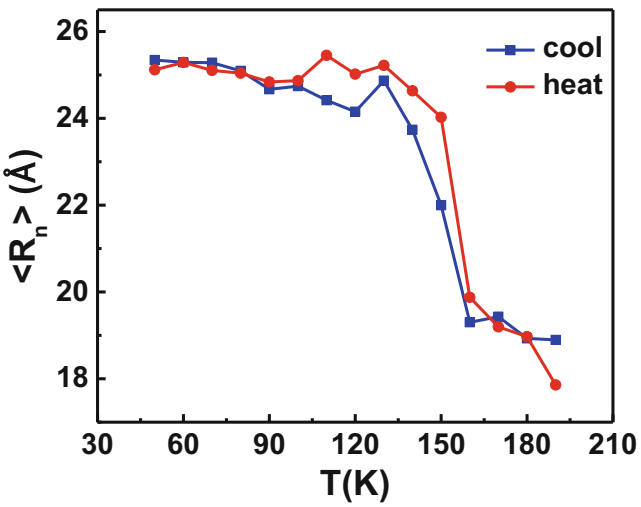

Fig. 9 Temperature dependence of the averaged end-to-end distance (<R_n>) during heating and cooling processes

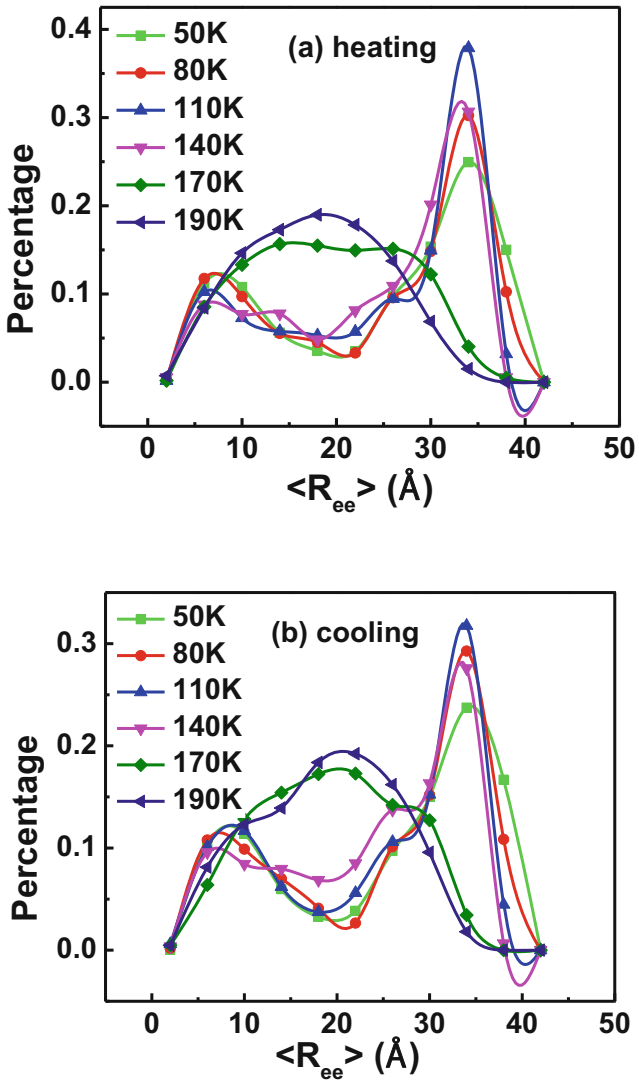

Fig. 10 Plots of chain end-to-end distributions for PE (15,166) cluster confined in SWNT during heating and cooling processes

heating and cooling processes in terms of the following relationship:

$$P_2 = \left\langle \frac{\langle 3\cos^2\theta - 1_{bond} \rangle}{2} \right\rangle, \quad (4)$$

where the inner brackets represent the average value for all sub-bonds of a system while the outer brackets display the time average. Usually, θ accounts for the angle between two sub-bond vectors (the sub-bond vector shows the vector obtained by connecting the center points of two neighboring

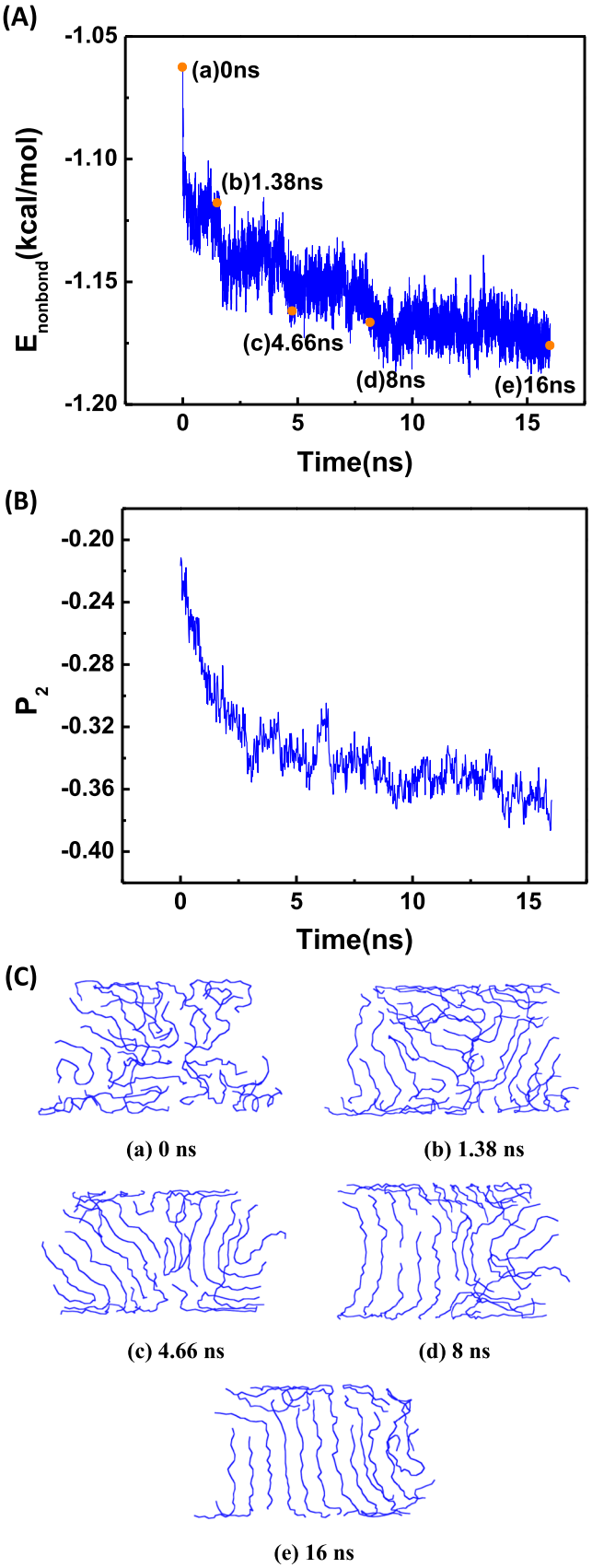

Fig. 11 The time dependence of nonbonded energy (**a**), global orientational order parameter P_2 (**b**), and outmost-layer structures (**c**) during quenching process of the confined PE (15,63) ▶

bonds). Martinez-Salazar [44] has defined θ as the angle between a sub-bond vector and z axis in the crystallization of free polyethylene. In the current work, as mentioned above, under the confined environment of SWNT, the completely ordered PE clusters adopt co-axial crystalline layer structures and the PE chains of each layer are parallel to each other and approximately perpendicular to the tube axis as shown in Fig. 5. Thus, here, we define θ as the angle between *a* sub-bond vector and the vector from the center of this sub-bond vector and tube center. The ordered conformations correspond to $P_2=-0.5$ ($\theta=90°$) instead of $P_2=1$, and completely disordered conformations correspond to $P_2=0$. Figure SI-5 reveals the temperature dependence of P_2 for PE polymers with different polymerization degree during heating and cooling processes. During heating process, the following features are observed from Fig. 7. First, within the temperature range lower than T_m, P_2 values are close to −0.45, which suggests that the PE cluster possesses ordered state within this temperature region. Second, around T_m, P_2-T curves exhibit sudden increase with increasing temperature, suggesting a considerable transformation from ordered state to disordered state. Third, at high temperature above T_m, the P_2 parameters are near −0.15, which reveals that the melted PE chains randomly distribute in SWNT within this temperature region.

As mentioned above, as shown in Figs. 4, 6, and 8, even in the melted PE cluster, there exists layering phenomenon, suggesting that layering is not the essential feature of liquid–solid phase transformation. With the purpose of revealing crystallization mechanism of confined PE clusters, the outmost-layer structures of PE (15,166) confined in (40,40)-SWNT at 170 and 140 K, respectively, are shown in Fig. SI-6. At 170 K, the outmost-layer of melted PE (15,166) cluster appears to be disordered (Fig. SI-6 (170 K)). However, at 140 K, the outermost-layer in solid PE (15,166) possesses ordered parallel-chain structure (Fig. SI-6 (a) (140 K)). In fact, their inner layers have similar structures. It reveals that transformation of disorder–order in each layer is a critical structure feature for the liquid–solid phase transition of confined PE (15, 166) cluster.

In order to demonstrate the time evolution of PE crystal growth, the melted PE (15,63) is quenched from 180 to 140 K for 16 ns. Figure 11 represents the time dependence of nonbonded energy, the global orientational order parameter P_2, and outmost-layer structures during the quenching process of the confined PE (15,63) cluster. As shown in Fig. 11, the nonbonded energy decreases with the time evolution (Fig. 11a), corresponding to the increasing of order degree (Fig. 11b). During 16 ns quenching process, crystalline layer gradually grows up, the PE chains cooperative orientation [3] and match each other. Finally, the ordered parallel-chain structure (Fig. 11c) is generated. In other words, after 16 ns quenching run, the outmost-layer of PE (15,63) cluster undergoes the disorder–order structure transformation.

Conclusions

To summarize, melting and freezing of PE clusters confined in (n,n)-SWNT are investigated by MD simulations with the united-atom force field for the interactions of PE and L-J potential for the UA-SWNT interactions. The global orientational order parameter P_2 is used to examine the order degree of whole polymer during heating and cooling processes. Importantly, the novel multishell structure of confined PE cluster is obtained in terms of structures and radial density distribution analyses, which can be ascribed to the confined environment provided by SWNT. The axis density distribution confirms that in solid PE cluster confined in (n,n)-SWNT, the PE chains of each layer are parallel to each other and approximately perpendicular to the tube axis. The nonbonded energies, structures, Lindemman index, radial density distributions, and diffusion coefficients with temperature reveal solid–liquid phase transition for confined PE clusters. Lindemman index analysis illustrates that the melting of PE cluster starts from inner layers. The chain end-to-end distribution curves for confined PE (15,166) adopt approximately Gaussian-like distribution above 150 K. Results demonstrate that the melting temperature increases with increasing of the polymerization degree as expected. The confined environment of SWNT significantly improves the thermal stability of PE cluster. Within three SWNTs with different chirality, similar multilayer structures are obtained, which is different from the results based on inducing crystallization out of tube. During quenching process of the confined PE clusters, the time evolution of the nonbonded energies, the global orientational order parameter P_2, and structures reveals that the crystal growth process is accomplished by disorder–order structure transformation in each layer of a confined PE cluster. Our work suggests SWNTs have a significant effect on the structures and stabilities of the confined PE clusters.

Acknowledgments This work is supported by grants from the National Science Foundation of China (Nos. 21276122, 21136001, and 91434109) and State Key Laboratory of Materials-Oriented Chemical Engineering, College of Chemistry and Chemical Engineering, Nanjing Tech University of China (No. ZK201212).

References

1. Hossain D, Tschopp MA, Ward DK, Bouvard JL, Wang P, Horstemeyer MF (2010) Molecular dynamics simulations of deformation mechanisms of amorphous polyethylene. Polymer 51:6071–6083
2. Van Krevelen DW, Nijenhuis KT (2009) Properties of polymers, 4th edn. Elsevier, Amsterdam
3. Yang JS, Yang CL, Wang MS, Chen BD, Ma XG (2011) Crystallization of alkane melts induced by carbon nanotubes and graphene nanosheets: a molecular dynamics simulation study. Phys Chem Chem Phys 13:15476–15482

4. Yamamoto T (2013) Molecular dynamics of polymer crystallization revisited: crystallization from the melt and the glass in longer polyethylene. J Chem Phys 139(054903):1–13
5. Yi P, Locker CR, Rutledge GC (2013) Molecular dynamics simulation of homogeneous crystal nucleation in polyethylene. Macromolecules 46:4723–4733
6. Ungar G, Stejny J, Keller A, Bidd I, Whiting MC (1985) The crystallization of ultralong normal paraffins: the onset of chain folding. Sci 229:386–389
7. Keller A (1957) A note on single crystals in polymers: evidence for a folded chain configuration. Philos Mag 2:1171–1175
8. Cormia RL, Price FP, Turnbull D (1962) Kinetics of crystal nucleation in polyethylene. J Chem Phys 37:1333–1340
9. Hoffman JD, Miller RL (1997) Kinetics of crystallization from the melt and chain folding in polyethylene fractions revisited: theory and experiment. Polymer 38:3151–3212
10. Tashiro K, Sasaki S (2003) Structural changes in the ordering process of polymers as studied by an organized combination of the various measurement techniques. Prog Polym Sci 28:451–519
11. Strobl G (2006) Crystallization and melting of bulk polymers: new observations, conclusions and a thermodynamic scheme. Prog Polym Sci 31:398–442
12. Schick C (2009) Differential scanning calorimetry (DSC) of semicrystalline polymers. Anal Bioanal Chem 395:1589–1611
13. Wang LZ, Duan LL (2012) Isothermal crystallization of a single polyethylene chain induced by graphene: a molecular dynamics simulation. Comput Theor Chem 1002:59–63
14. Wei CY (2007) Structural phase transition of alkane molecules in nanotube composites. Phys Rev B: Condens. Matter Mater Phys 76:134104 1–10
15. Wei CY (2009) Adsorption of an alkane mixture on carbon nanotubes: selectivity and kinetics. Phys Rev B Condens Matter Mater Phys 80(085409):1–7
16. Li LY, Li CY, Ni CY (2006) Polymer crystallization-driven, periodic patterning on carbon nanotubes. J Am Chem Soc 128:1692–1699
17. Wang BB, Li B, Xiong J, Li CY (2008) Hierarchically ordered polymer nanofibers via electrospinning and controlled polymer crystallization. Macromolecules 41:9516–9521
18. Li B, Li LY, Wang BB, Li CY (2009) Alternating patterns on single-walled carbon nanotubes. Nat Nanotechnol 4:358–362
19. Hu X, An HN, Li ZM, Geng Y, Li LB, Yang CL (2009) Origin of carbon nanotubes induced poly(L-Lactide) crystallization: surface induced conformational order. Macromolecules 42:3215–3218
20. Yang H, Chen Y, Liu Y, Cai WS (2007) Molecular dynamics simulation of polyethylene on single wall carbon nanotube. J Chem Phys 127(094902):1–6
21. Ramanathan T, Abdala AA, Stankovich S, Dikin DA, Herrera-Alonso M, Piner RD, Adamson DH, Schniepp HC, Chen X, Ruoff RS, Nguyen ST, Aksay IA, Prud'Homme RK, Brinson LC (2008) Functionalized graphene sheets for polymer nanocomposites. Nat Nanotechnol 3:327–331
22. Eslami H, Rahimi M, Muller-Plathe F (2013) Molecular dynamics simulation of a silica nanoparticle in oligomeric poly(methyl methacrylate): a model system for studying the interphase thickness in a polymer−nanocomposite via different properties. Macromolecules 46:8680–8692
23. Eslami H, Behrouz M (2014) Molecular dynamics simulation of a polyamide-66/carbon nanotube nanocomposite. J Phys Chem C 118: 9841–9851
24. Xu JZ, Chen T, Yang CL, Li ZM, Mao YM, Zeng BQ, Hsiao BS (2010) Isothermal crystallization of poly(l-lactide) induced by graphene nanosheets and carbon nanotubes: a comparative study. Macromolecules 43:5000–5008
25. Cheremisinoff NP (1996) Polymer characterization: laboratory techniques and analysis, 1st edn. Noyes, Westwood
26. Zhang XB, Li ZS, Lu ZY, Sun CC (2001) Molecular dynamics simulation of the linear low-density polyethylene crystallization. J Chem Phys 115:3916–3922
27. Plimpton S (1995) Fast parallel algorithms for short-range molecular dynamics. J Comput Phys 117:1–19
28. Shimizu T, Yamamoto T (2000) Melting and crystallization in thin film of n-alkanes: a molecular dynamics simulation. J Chem Phys 113:3351–3359
29. Hwang HJ, Kwon OK, Kang JW (2004) Copper nanocluster diffusion in carbon nanotube. Solid State Commun 129:687–690
30. Arcidiacono S, Walther JH, Poulikakos D, Passerone D, Koumoutsakos P (2005) Solidification of gold nanoparticles in carbon nanotubes. Phys Rev Lett 94(105502):1–4
31. Harmandaris VA, Mavrantzas VG, Theodorou DN (1998) Atomistic molecular dynamics simulation of polydisperse linear polyethylene melts. Macromolecules 31:7934–7943
32. Guo ZX, Ding JW, Xiao Y, Mao YL (2006) Lattice dynamics of carbon chain inside a carbon nanotube. J Phys Chem B 110:21803–21807
33. Waheed N, Lavine MS, Rutledge GC (2002) Molecular simulation of crystal growth in n-eicosane. J Chem Phys 116:2301–2309
34. Ko MJ, Waheed N, Lavine MS, Rutledge GC (2004) Characterization of polyethylene crystallization from an oriented melt by molecular dynamics simulation. J Chem Phys 121:2823–2832
35. Huang JF, Zhu XL, Bartell LS (1998) Molecular dynamics studies of the kinetics of freezing of $(NaCl)_{108}$ clusters. J Phys Chem A 102: 2708–2715
36. Stack GM, Mandelkern L, Voigt-Martin IG (1984) Crystallization, melting, and morphology of low molecular weight polyethylene fractions. Macromolecules 17:321–331
37. Sun CQ, Shi Y, Li CM, Li S, Au Yeung TC (2006) Size-induced undercooling and overheating in phase transitions in bare and embedded clusters. Phys Rev B 73(075408):1–9
38. Stubbs JM, Potoff JJ, Siepmann JI (2004) Transferable potentials for phase equilibria. 6. United-atom description for ethers, glycols, ketones, and aldehydes. J Phys Chem B 108:17596–17605
39. Yamamoto T (2005) Molecular dynamics modeling of the crystal-melt interfaces and the growth of chain folded lamellae. Adv Polym Sci 191:37–85
40. Alavi S, Thompson DL (2006) Molecular dynamics simulations of the melting of aluminum nanoparticles. J Phys Chem A 110:1518–1523
41. Durand M, Meyer H, Benzerara O, Baschnagel J, Vitrac O (2010) Molecular dynamics simulations of the chain dynamics in monodisperse oligomer melts and of the oligomer tracer diffusion in an entangled polymer matrix. J Chem Phys 132(194902):1–10
42. Tseng HC, Chang RY, Wu JS (2011) Molecular structural property and potential energy dependence on nonequilibrium-thermodynamic state point of liquid n-hexadecane under shear. J Chem Phys 134(044511):1–13
43. Wang XL, Lu ZY, Li ZS, Sun CC (2007) Molecular dynamics simulation study on controlling the adsorption behavior of polyethylene by fine tuning the surface nanodecoration of graphite. Langmuir 23: 802–808
44. Ramos J, Martinez-Salazar J (2011) Computer modeling of the crystallization process of single-chain ethylene/1-hexene copolymers from dilute solutions. J Polym Sci Part B Phys 49:421–430